Influence of Thermo-Oxidative Aging on Vibration Damping Characteristics of Conventional and Graphene-Based Carbon Fiber Fabric Composites

Wei Fan, Jia-lu Li, Lei Chen, Huan Wang, Dan-dan Guo, Jing-xue Liu
Composite Research Institute of Tianjin Polytechnic University, Tianjin and Education Ministry Key Laboratory of Advanced Textile Composite Materials, Tianjin 300387, China

The effect of thermo-oxidative aging on the vibration damping characteristics of the conventional fabric composites reinforced by three-dimensional (3D) and four-directional (4Dir) braided preform and laminated plain woven fabric and the 3D-4Dir braided graphene-based carbon fiber composites was investigated. Specimens were isothermally aged at 140 °C for various periods of time up to 1,200 h. The results indicated that the thermo-oxidative aging resulted in deterioration of the matrix and interface performance, in the form of chain scissions, weight loss, microcracks and interfacial debonding, which should be responsible for the decrease of nature frequency and the increase of damping coefficient of the composites. After aging for 1,200 h, the first nature frequency and first damping coefficient retention rates of 3D-4Dir braided graphene-coated carbon fiber/epoxy composite were 5.5% and 6.4% higher than those of laminated composite, respectively. One of the reasons was the integrated structure of 3D-4Dir braided composite exposed lower fiber end area to air than that of laminated composite, leading to less interface oxidation. Another reason was that the graphene reinforced gradient interphase provided an effective shield against interface oxidation and restricted the movement of the different phase of the materials at the composites interface. This synergetic reinforcing effect of 3D-4Dir braided structure and graphene reinforced hierarchical interface provides an easy and effective way to design and improve the thermo-oxidative stability of carbon fiber reinforced polymer composites. POLYM. COMPOS., 00:000–000, 2015. © 2015 Society of Plastics Engineers

INTRODUCTION

Carbon-fiber-reinforced polymers composites (CFRPCs) are largely employed in the aerospace industry because of their high specific mechanical properties [1–3]. In the next future CFRPCs are expected to be employed in structural parts subjected to rather severe thermal conditions. Under such conditions oxidation reaction/diffusion phenomena take place within the CFRPCs and result in the deterioration of the matrix (such as weight loss, embrittlement, and chain scissions) and the fiber/matrix interfaces [4–6]. For the conventional laminated composites, the occurrence and the development of microscopic damage (fiber/matrix debonding or microcracks) give rise to the onset of oxidized/damaged layers. This process is prone to drilling-induced delamination. By contrast, three-dimensional (3D) braided composites show low delamination tendency in combination with near-net-shape manufacturing, out-of-plane stiffness, high strength, and impact tolerance as well as anti-ablation resistance [7]. However, little research has been performed to investigate the thermo-oxidative aging (TOA) effect on the 3D braided composites.

Previous research has shown that CFRPCs with higher interface bonding performance have higher thermo-oxidative stability [8]. In recent years, the introduction of graphene nanoplatelet (GN) into conventional continuous fiber-reinforced polymer composites to create hierarchical reinforcement structures is a current topic of interest because of the unique structures, outstanding strength and modulus, excellent electrical and thermal properties of the GN [1, 9]. It has been demonstrated that by adopting the multiscale reinforcements, significant improvements are achieved in CFRPCs, especially for the fiber/matrix interphase and matrix-dominated out-of-plane performances, such as interfacial shear strength [1, 10], impact strength [1], and fatigue resistance [9]. However, there are few studies regarding the property of GN reinforced CFRPCs after TOA.

The vibration damping characteristics are very important for CFRPCs because these materials are often applied to systems exposed to external impact and periodic loading [11]. In the past 40 years, a lot of studies [4, 6, 8, 12] have been performed to investigate the effect of TOA on

Correspondence to: Jia-lu Li; e-mail: lijialu@tjpu.edu.cn
Contract grant sponsor: Tianjin Municipal Science and Technology Commission, China; contract grant numbers: 10SYSYJC27800 and 11ZCKFSF00500.
DOI 10.1002/pc.23484
Published online in Wiley Online Library (wileyonlinelibrary.com).

the mechanical properties of CFRPCs. However, no research has been reported on the effect of TOA on their vibration damping characteristics.

The purpose of the current investigation was to identify the effect of TOA on the vibration damping characteristics of CFRPCs and determine the role of reinforced structure (3D and four-directional (4Dir) braiding preform and laminated plain woven fabric) and GN reinforced hierarchical interface on the vibration damping characteristics of CFRPCs before and after TOA. Therefore specimens were thermally oxidized at 140 °C for various durations. After exposure to the high temperature, composites are characterized to: (1) determine their weight loss and changes in dynamic mechanical properties and vibration damping characteristics at different exposure times; (2) observe the corresponding microcracks and surface damage; (3) understand the reinforced mechanism using the different reinforced structure and the GN reinforced hierarchical interface.

EXPERIMENTAL DETAILS

Materials

Commercially available, T700-12K carbon fibers (Toray) and plain-weave T700-12K carbon fiber fabric with areal density of 400 g/m^2 and the warp and weft densities of 2.5 yarns/cm (Yi Xing New Carbon Fiber Weaving) were used for this study. An epoxy resin JC-02A based on diglycidyl ether of bisphenol A (Changshu Jaffa Chemical) with hardener JC-02B (improved methyl tetrahydrophthalic anhydride) and accelerant JC-02C (tertiary amine) were used as matrix. Graphite powders with an average diameter of 10 μm were purchased from Qingdao AoKe ShiMo, China. Concentrated H_2SO_4 (98%), concentrated H_3PO_4 (85%), $KMnO_4$, acetone and 30% H_2O_2 (Tianjin Feng Chuan) were used to make GN.

Preparation of GN

Graphite oxide (GO) was synthesized with a Marciano's method [13, 14]. A 9:1 mixture of concentrated H_2SO_4/H_3PO_4 (360:40 ml) was added to a mixture of graphite powders (3.0 g, 1 wt equiv) and $KMnO_4$ (18.0 g, 6 wt equiv), producing a slight exotherm to 35–40 °C. The mixture was stirred for 12 h at 50 °C, forming a thick paste. Subsequently, it was cooled to room temperature and poured onto ice (400 ml) with 30% H_2O_2 (3 ml). The remaining solid materials were then washed in succession with deionized water until pH was 7. Finally, they were dried at vacuum freeze drier for 12 h to get GO. The dry GO was grinded into powder. GN was produced by the thermal exfoliation [9] of GO. Placed GO powder (200 mg) in a quartz boat and put the quartz boat carefully into the vacuum/atmosphere tube furnace (SK-1,400 °C, Central Laboratory Electric Furnace, Tianjin, China) preheated to 1,050 °C and held in the furnace for ~35 s. Took out the quartz boat, the black flocculent material was the GN.

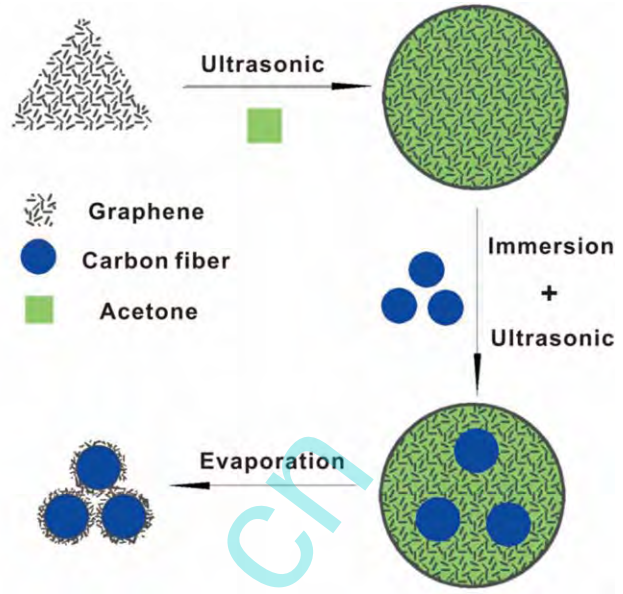

FIG. 1. Schematic of the graphene-depositing process on carbon fibers. [Color figure can be viewed in the online issue, which is available at wileyonlinelibrary.com.]

Preparation of GN-Coated Fibers

The GN were dispersed in acetone, and sonicated for 2 h to obtain the stable suspension of 1 mg ml^{-1}. It should be noted that the temperature was controlled at room temperature in the whole process of sonication step. After that, the T700-12K carbon fibers which had been weighed were soaked in the homogeneous mixtures for 20 s to absorb the solutions containing GN. Then these carbon fibers coated by GN were dried at 50 °C under vacuum and the weight of carbon fibers was measured again. The weight of GN was calculated by changes in weight of carbon fibers. Then these steps were repeated until the contents of GN in composites reached 1 wt%. The weight of GN in the composite was chosen as 1% because the previous work has proved that this content is the best proportion to improve the fiber/matrix interface performance at room temperature [15]. The production procedure of the GN-coated fibers is illustrated in Fig. 1.

Preparation of Conventional and Graphene-Based Carbon Fiber Fabric Composites and Neat Resin

Table 1 shows the complete names and abbreviations of the conventional and graphene-based carbon fiber fabric composites and neat resin. Both the 3D-4Dir braided raw carbon fiber preforms and 3D-4Dir braided GN-coated carbon fibers preforms were manufactured by 4-Step 3D braiding process [16]. The 3D-4Dir braided

DOI 10.1002/pc

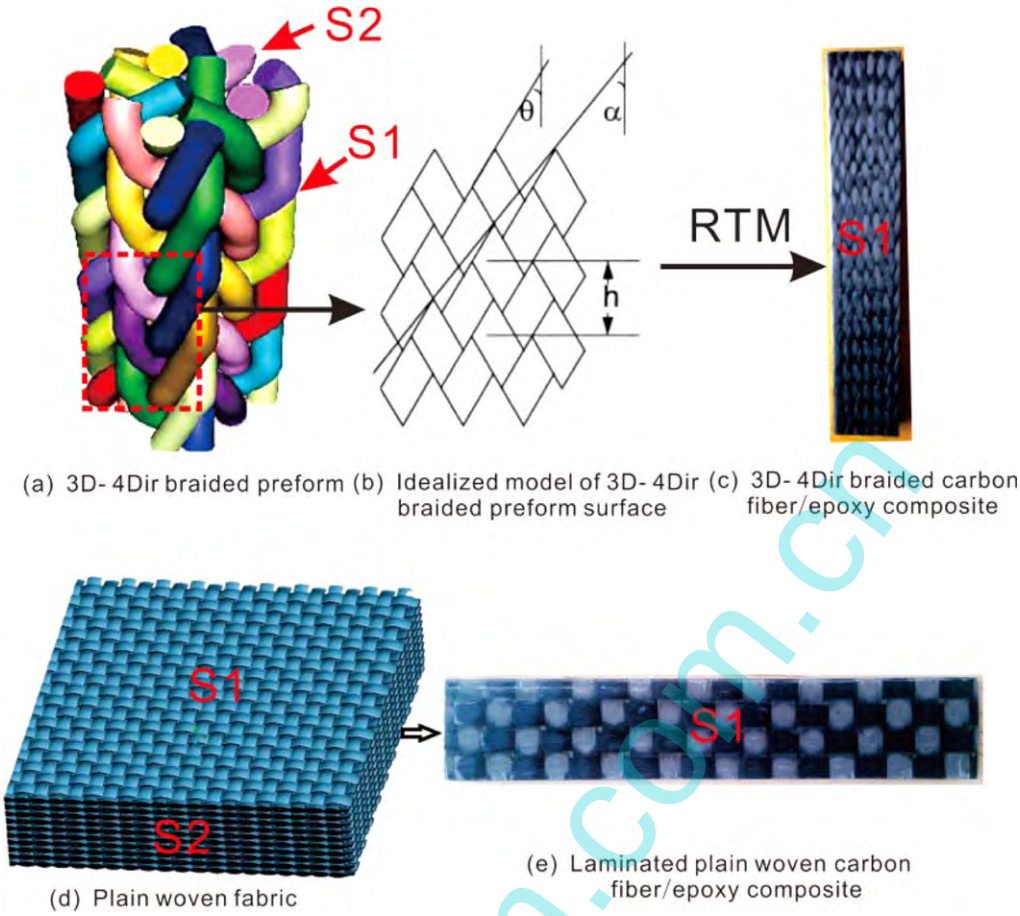

FIG. 2. (a) Reinforced structure diagram of BC, (b) an idealized model of the 3D-4Dir braided perform surface, (c) the BC sample, (d) the reinforced structure diagram of LC, and (e) the LC sample. S_1 =Area of non-machined resin-rich surfaces and S_2 = Area of surfaces cut perpendicular to fibers. [Color figure can be viewed in the online issue, which is available at wileyonlinelibrary.com.]

architecture is illustrated in Fig. 2a. It is characterized by almost all braider yarns being offset at different angles between the in-plane and through-thickness directions, which can be seen clearly from the tracer yarn (colored yarns). An idealized model of the braided preform surface is shown in Fig. 2b, where h is the braiding pitch length, θ is the surface braiding angle, and α is the braiding angle. The average braiding angle α of BC and BGC in this article was 22.3°. The laminated plain woven fabric is illustrated in Fig. 2d. The production process of BGC was the same as the BC, just the fiber used for BGC was the GN-coated fibers. The making process of the composites and the neat resin is covered elsewhere [4]. Final specimens of the BC and LC are illustrated in Fig. 2c and e, respectively. The fiber volume fractions for different composites were about 55%.

TABLE 1. The complete names and abbreviations of the conventional and graphene-based carbon fiber fabric composites and neat resin.

Abbreviation	Complete name
BC	3D-4Dir braided carbon fiber/epoxy composites
BGC	3D-4Dir braided GN-coated carbon fibers/epoxy composites
LC	Laminated plain woven carbon fiber/epoxy composites
NR	Neat resin

Accelerated Aging Experiments

In order to evaluate the effect of TOA on the vibration damping characteristics of CFRPCs, an accelerated TOA procedure was adopted in accordance with GB/T 2573-2008. Specimens were isothermally aged at 140 °C for 168, 360, 720, and 1,200 h. After heating at a given aged time, specimens were removed, cooled in a desiccator to avoid moisture absorption. The specimens must be stored at 25±3 °C for at least 24 h prior to test.

Characterization

The surface topography of carbon fiber and the cross-section of composite specimens were obtained on a Hitachi S-4800 FE-SEM (operated at 4 kV). The specimens were coated with a conductive layer of gold. The force modulation mode of AFM (CSPM 5500 atomic force

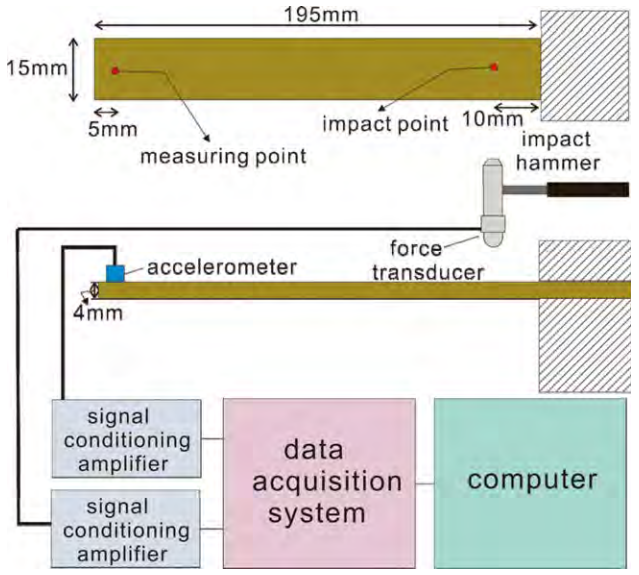

FIG. 3. Experimental setup for forced vibration of a cantilever beam. [Color figure can be viewed in the online issue, which is available at wileyonlinelibrary.com.]

microscopy) is adopted to study the stiffness of various phases of composites.

Thermal conductivity of the composites was examined by TC 3010 apparatus (Xi'an Xiatech Electronic Technology, China) according to ASTM C1113/C1113M-09. The testing specimens had dimensions of 40 mm × 30 mm × 4 mm.

Changes in the composition of the polymer matrix were analyzed by micro-attenuated total reflection Fourier transform infrared spectroscopy (FTIR) [17]. Data acquisition was performed automatically using an object-oriented computer and a standard software package.

An electronic balance with 0.1 mg accuracy was used for recording the weight loss of composites. The damping specimens were first used to measure the weight loss. Dynamic mechanical analysis (DMA) was conducted on the specimens according to ASTM E1640-2009 with a three-point bending mode to investigate the storage modulus (E'), loss modulus (E''). The tests were performed in the scanning temperature mode, in the range from 40 °C to 185 °C, at a heating rate of 5 °C/min, and with an oscillating frequency of 1.0 Hz. Three specimens of rectangle shape with a nominal size of 60 mm × 10 mm × 2 mm were analyzed for each level of thermal treatment.

Photomicrograph of the LC, BC, and BGC specimens was carried out by means of a VHX-1000 three-dimensional microscopy systems and FE-SEM. A JEOL TM-100 SEM was employed to observe fiber–matrix interfaces of the composites.

Modal analysis was performed with the help of an impact hammer test. The vibration damping characteristics of the composites were measured by the setup shown in Fig. 3. One end (25 mm) of a damping specimen was clamped into a custom-made. The damping specimen was excited by an impact hammer (BZ1201) at a position 10 mm from the clamp and the resulting vibrations were measured at a position 5 mm from its free-end by a miniature pick-up accelerometer (LC0408T). The input force signal and the output acceleration signal were fed to a dual channels power amplifier (WS2401) and AD converter (WS5921), respectively. The signals were analyzed by the modal software (Vib' SYS modal analysis system) to get the first modal parameters (frequency response function, natural frequency, damping ratio) of the beam.

RESULTS

Surface Topography and Stiffness Distribution of the Hierarchical Interphase

To verify the introduction of hierarchical layer, the interfacial phase structures of the pristine and the multiscale composites loading with 1 wt% GN were detected in detail. Figure 4a is the surface morphologies of the raw carbon fiber, indicating T700 carbon fiber had a smooth surface. Figure 4b is a schematic representation of the unit cell that constitutes the 2-phase (carbon fiber/epoxy) composite (BC). Figure 4c is a FE-SEM image of cross-section of the BC. Figure 4d is the carbon element content varying from carbon fiber to epoxy along the direction of red arrow in Fig. 4c delivered by FE-SEM/energy dispersive spectrometer (EDS). It can be seen that the carbon element content had a sudden drop from the carbon fiber to the epoxy resin (Fig. 4d), indicating that carbon element content in epoxy resin was significantly less than in carbon fiber. Figure 4e shows the relative stiffness images of cross-section areas in the BC measured by AFM. The relative stiffness image of carbon fibers was brighter than the surrounding epoxy, which meant that the stiffness of carbon fiber was higher than epoxy. Besides, it demonstrated that the relative stiffness image displayed a clear distinction between carbon fiber and the surrounding epoxy (Fig. 4e). Figure 4f is the relative stiffness distribution curve from carbon fiber to epoxy resin along the direction of dash line in Fig. 4e. The vertical axis of Fig. 4f denotes the relative stiffness value which was indirectly indicated by the voltage generated from the cantilever deflection of AFM. The stiffness decreased significantly from carbon fiber to epoxy (Fig. 4f), which clearly indicated that there were two stiffness phases representing carbon fiber and epoxy in the composite interface and no transition phase about hardness.

The typical FE-SEM image of the GN-deposited carbon fiber is shown in Fig. 5a. It can be seen that most GN attached to the fiber surface, which identified that a new hierarchical structure was formed. Figure 5b is a schematic representation of the unit cell that constitutes the 3-phase (carbon fiber/graphene/epoxy) hierarchical composite (BGC). Figure 5d is the carbon element content varying from carbon fiber to epoxy corresponding to Fig. 5c delivered by SEM/EDS. It can be seen that carbon element content dwindled steadily from carbon fibers to epoxy, which indicated the gradient distribution of GN in the BGC and

DOI 10.1002/pc

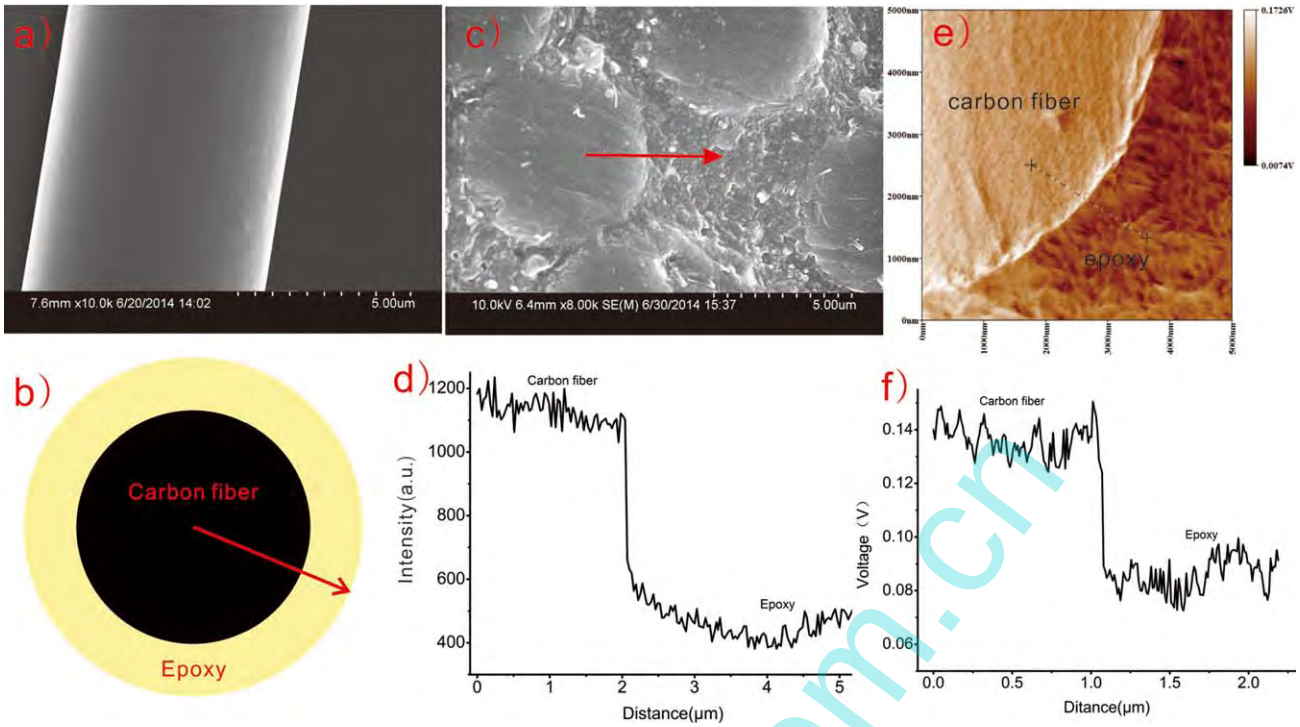

FIG. 4. (a) The surface morphologies of the raw carbon fiber. (b) Schematic representation of the unit cell that constitutes the 2-phase (carbon fiber/epoxy) composite (BC). (c) FE-SEM image of cross-section of the BC. (d) Carbon element content varying from carbon fibers to epoxy along the direction of arrow in (c). (e) Relative stiffness image of cross-section areas of the BC. (f) Relative stiffness distribution curve from carbon fiber to epoxy resin along the direction of dash line in (e). [Color figure can be viewed in the online issue, which is available at wileyonlinelibrary.com.]

supported the construction of gradient interface layers with a thickness of ~0.98 μm. Figure 5e shows the relative stiffness images of cross-section areas in BGC. The boundary of carbon fiber and epoxy became blurrier. Figure 5f is the relative stiffness distribution curve from carbon fiber to epoxy resin along the direction of dash line in Fig. 5e. It can be seen that stiffness decreased gradually from the carbon fiber to epoxy, which implied the introduction of gradient interface layer and was in good agreement with the linear FE-SEM results. The interphase thickness value was ~0.94 μm in Fig. 5f, which was a little smaller than that in Fig. 5d because of disparity of specimens and experimental errors.

Thermal Conductivity

Figure 6 shows that the thermal conductivity of the NR, BC, and BGC was 0.18, 0.91, and 1.03 W/(m·k), respectively. It should be noted that the thermal conductivities of the BC and BGC in this paper were along the width of the specimens.

Chemical Analysis

The representative FTIR spectra of NR samples after aging at 140 °C for different aging times are shown in Fig. 7. It can be seen that the characteristic band of C=O near 1,730 cm^{-1} increased with the decrease of the band of C-H near 2,922 and 2,851 cm^{-1}. The phenomena demonstrated that C-H bonds were oxidized and saturated aldehyde, ketone, ester, or acid was formed [17, 18]. In addition, the characteristic absorption bands of benzene ring near 1,606, 1,508, and 1,456 cm^{-1} decreased in intensity with aging process, which is because the benzene ring structure was partly destroyed, and chemical species, O=(C_6H_4)=O (a 'black-color' element), were formed [19]. The absorption band near 1,178 cm^{-1}, which derived from symmetrically stretching vibration of C-O-phenyl, decreased in intensity with the aging process. These results indicated that part of C-O-phenyl were destroyed [18]. The intensity of carbonyl and C-H bonds did not appear to have obvious change from 720 to 1,200 h of the aging time. There may be two reasons for this phenomenon. Firstly, further oxidation of the carbonyl species was likely to form CO_2 with the aging proceeds [19]. Secondly, ketone formation yielded a structure more resistant to oxidation [20].

Weight Loss

Figure 8 illustrates the measured weight loss of the three composites at 140 °C as a function of aging time. It can be seen that the weight loss all increased with longer aging times. Besides, the weight loss of LC was about 1.3

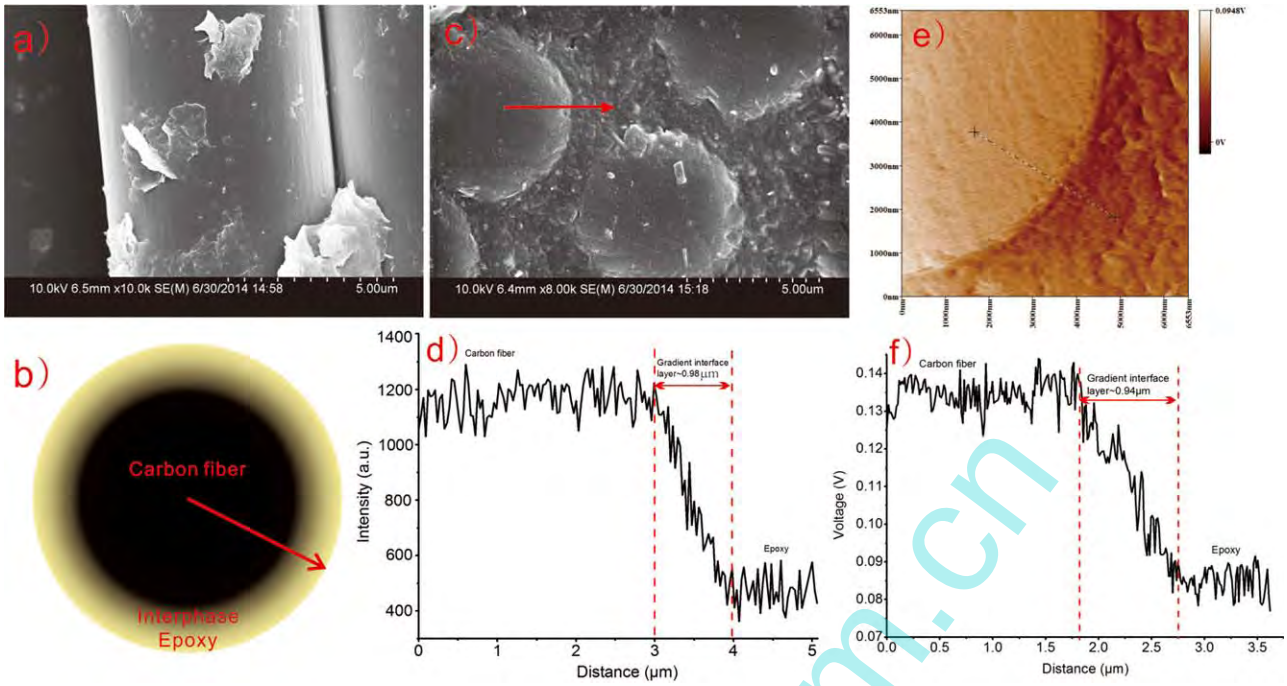

FIG. 5. (a) The surface morphologies of the graphene-deposited carbon fibers. (b) Schematic representation of the unit cell that constitutes the 3-phase (carbon fiber/graphene/epoxy) hierarchical composite (BGC). (c) FE-SEM image of cross-section of the BGC. (d) Carbon element content varying from carbon fibers to epoxy along the direction of arrow in (c). (e) Relative stiffness image of cross-section areas of the BGC. (f) Relative stiffness distribution curve from carbon fiber to epoxy resin along the direction of dash line in (e). [Color figure can be viewed in the online issue, which is available at wileyonlinelibrary.com.]

and 1.8 times as high as that of BC and BGC, respectively.

Thermomechanical Property

The chemical and physical aging occurred during aging and accompanied by a variation in molecular mobility. These variations were accounted for by monitoring the E' and E''. The results obtained using the DMA curves for BC are presented in Fig. 9. From Fig. 9, it can be seen that the E' decreased (Fig. 9a) and E'' increased (Fig. 9b) with longer aging times. The trends of DMA traces were similar for the BC, LC, and BGC, therefore, only one set of them were presented in Fig. 9.

Fracture Behavior

Figure 10 shows the cross-section photomicrograph of LC specimens aged at 140 °C for 1,200 h compared to

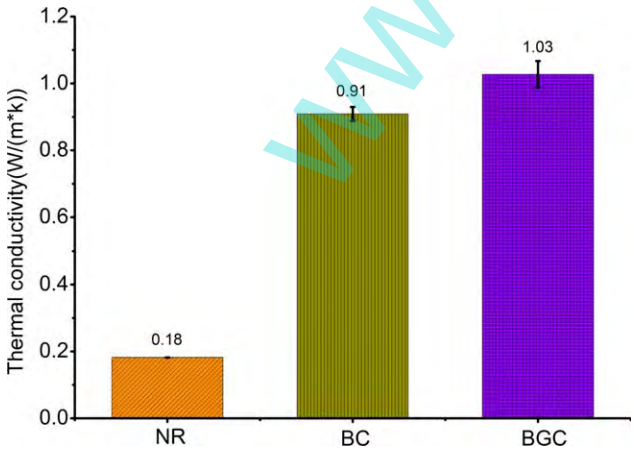

FIG. 6. Thermal conductivity of NR, BC, and BGC. [Color figure can be viewed in the online issue, which is available at wileyonlinelibrary.com.]

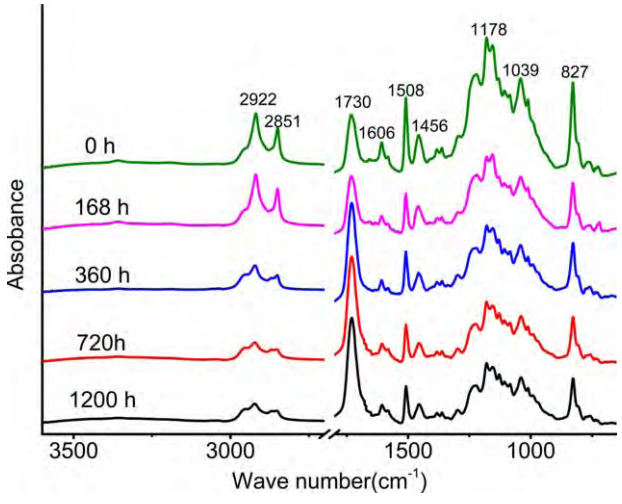

FIG. 7. FTIR spectra of NR samples after aging at 140 °C for different aging times. [Color figure can be viewed in the online issue, which is available at wileyonlinelibrary.com.]

DOI 10.1002/pc

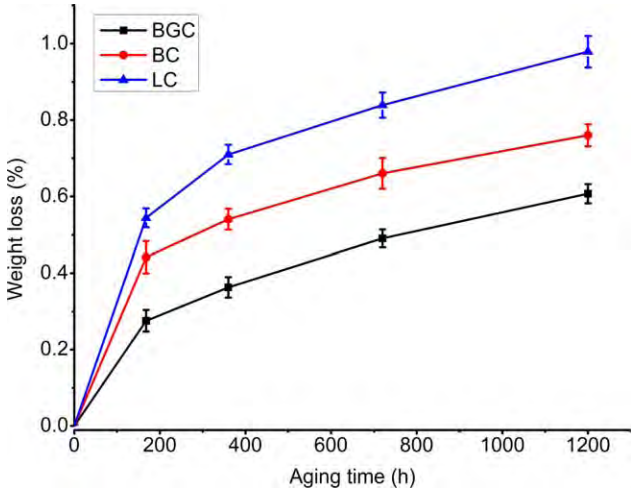

FIG. 8. Weight loss vs. aging time for specimens aged at 140 °C. [Color figure can be viewed in the online issue, which is available at wileyonlinelibrary.com.]

unaged one. No damage was observed on the unaged specimen surface (Fig. 10a). However, a lot of microcracks appeared on the aged specimen (Fig. 10b). The microcracks largely appeared on the fiber end areas and few on the areas parallel to the fiber (Fig. 10c), and some microcracks even seem to have developed into delamination (Fig. 10d). Figure 11 shows the cross-section photographs of BC and BGC specimens aged at 140 °C for 1,200 h compared to unaged one. For the BC, no damage was observed on the unaged specimen surface (Fig. 11a). TOA induced matrix shrinking and fiber/matrix debonding onset was observed on the end cross-section of the aged specimen (Fig. 11b). The microcracks and matrix shrinking were also noted on the end cross-section of BGC (Fig. 11c). However, in comparison to the BC, the extent of microcracks was much less in BGC specimens. By comparing Fig. 11d and e, it can be seen that microcracks in BC were more open than in BGC, and the fiber/matrix debonding onset (Fig. 11d) was observed clearly.

Figure 12 shows the typical SEM pictures of the fracture surfaces of unaged and aged BC (left) and BGC (right). The fracture surfaces were similar for both BC and LC, therefore, only one set of them were presented in Fig. 12. On fracture surfaces of both unaged specimens, fibers were covered with the matrix representing a good adhesion between fiber and matrix. In aged BC specimens, the microcracks propagated almost entirely along the fiber/matrix interface after 168 h of TOA (Fig. 12b); the grooves were formed because of the pull out of fibers after 360 h of TOA (Fig. 12c); with the aging time increasing, the fibers were lying loosely and the fiber surfaces were completely devoid of matrix resin (Figs. 12d and e). Significant interfacial failure was also noted in the fracture surfaces of BGC. However, the degree of the interface damage in BGC was not as serious as that of BC. The fibers on the fracture surfaces of BGC specimens were still held together by the matrix resin after 720 h of TOA (Fig. 12I). Although the fibers were lying loosely after 1,200 h of TOA (Fig. 12J), the matrix resins were still present, filling the space between the fibers. The photomicrographs and SEM analyses illustrated that the GN/epoxy interface layer in BGC can provide an effective shield against oxidation.

Vibration Damping Characteristics

Based on the experimental frequency response functions curves, the nature frequency and damping coefficient values (achieved by the half-power band width method [21]) of composites could be extracted. Figure 13a and b present the first nature frequency (FNF) and the first damping coefficient (FDC) results of the three unaged composites. The FNF of BGC (99.01 Hz) was greater than that of BC (93.98 Hz) and LC (69.37 Hz). In contrast, the FDC of BGC (1.85%) was less than that of BC (1.98%) and LC (2.46%).

The effect of aging time on the FNF and FDC of the three composites is shown in Figs. 14 and 15,

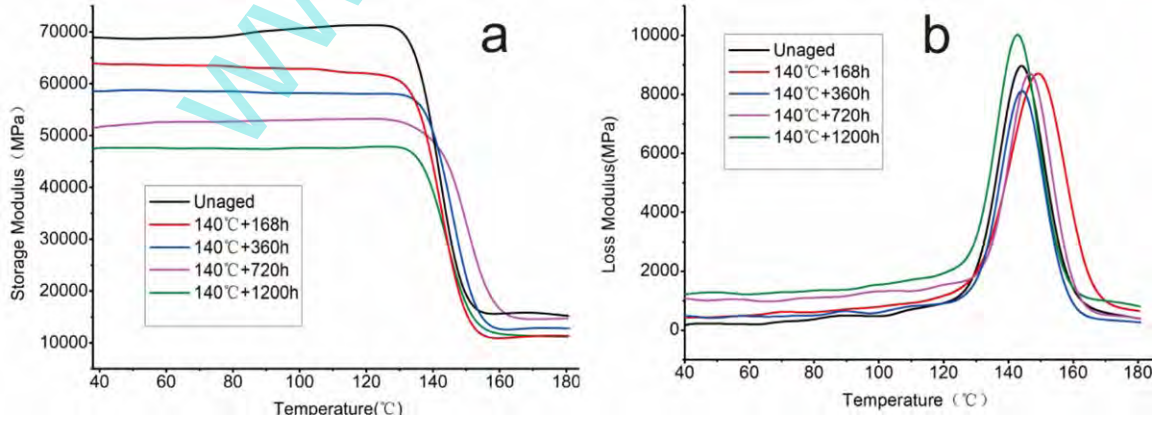

FIG. 9. (a) Storage modulus and (b) loss modulus vs. aging time for specimens aged at 140 °C. [Color figure can be viewed in the online issue, which is available at wileyonlinelibrary.com.]

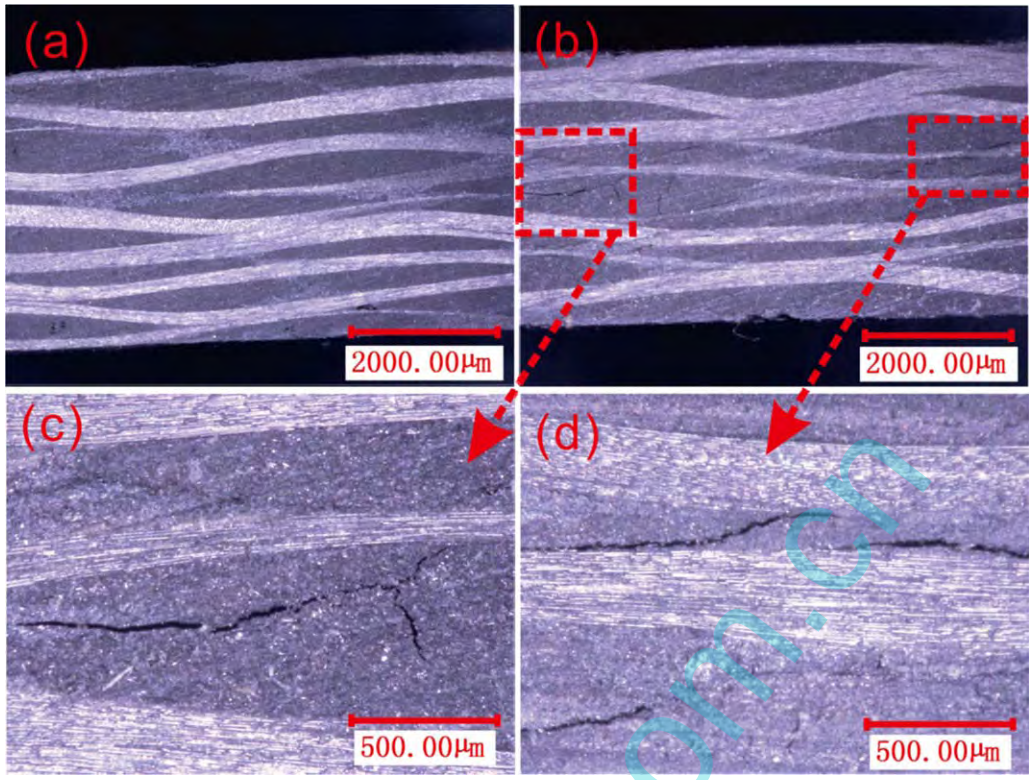

FIG. 10. Photomicrographs of cross-section of (a) unaged and (b) aged (1200 h at 140 °C) LC; Zoom on thermo-oxidation induced microcracks (c and d). [Color figure can be viewed in the online issue, which is available at wileyonlinelibrary.com.]

respectively. It can be seen that the FNF decreased and the FDC increased with the increasing of aging time for the three composites. The decrease in FNF (Fig. 14d) and the increase in FDC (Fig. 15d) of LC were higher than those of BC and BGC. For example, after aging for 1,200 h, the decrease in FNF of LC (7.3%) was higher than that of BC (4.4%) and BGC (1.8%), and the increase in the FDC of LC (28.6%) was higher than that of BC (26.3%) and BGC (22.2%). In other words, the FNF retention rates of BC and BGC were 2.8% and 5.5% higher than that of LC, respectively. The FDC retention rates of BC and BGC were 2.3% and 6.4% higher that of LC, respectively.

DISCUSSION

Interpretation of Weight Loss by Reinforced Structure and GN Reinforced Gradient Interface

In the case of CFRPCs, weight loss was (in general) associated only with the polymer, as the reinforced carbon fiber was thermally stable at 140 °C [19]. In this research, the LC and BC specimens owned the same matrix resin content (45%), so they should have the same weight loss. The weight loss of the two composites did not appear to follow the expected behavior with the weight loss of BC equal to that of the LC, however, the LC lost considerably more weight than BC under the same aging conditions. Previous works [6, 22] indicate that a specimen with higher percentage of fiber end area exposed to air is more susceptible to lead interface oxidation, resulting in more weight loss. In this article, the weight loss data presented were an average of the values obtained from the damping specimens, so the surface area ratio $S_2/(S_1+S_2)$ for LC and BC was 22% and 1.4%, respectively. However, the plain weave fabric only had half of the fibers perpendicular to S_2, so the actual ratio of fiber end area to the total surface area in LC was 11%, which was about 7.9 times higher than that of BC. Therefore, the LC lost more weight than BC. The weight loss of BC was bigger than that of BGC, which was because the BGC with the gradient interface layer had a good fiber to matrix adhesion, providing an effective shield against interface oxidation. The interfacial reinforcing mechanism by the GN will be discussed in the following.

Interpretation of Vibration Damping Characteristics by Reinforced Structure and GN Reinforced Gradient Interface

The relationship between the nature frequency and Young's modulus is fit for Meirovich's continuous beam model [23]. In this theory, the natural frequency of the first cantilever beam mode can be written as

 DOI 10.1002/pc

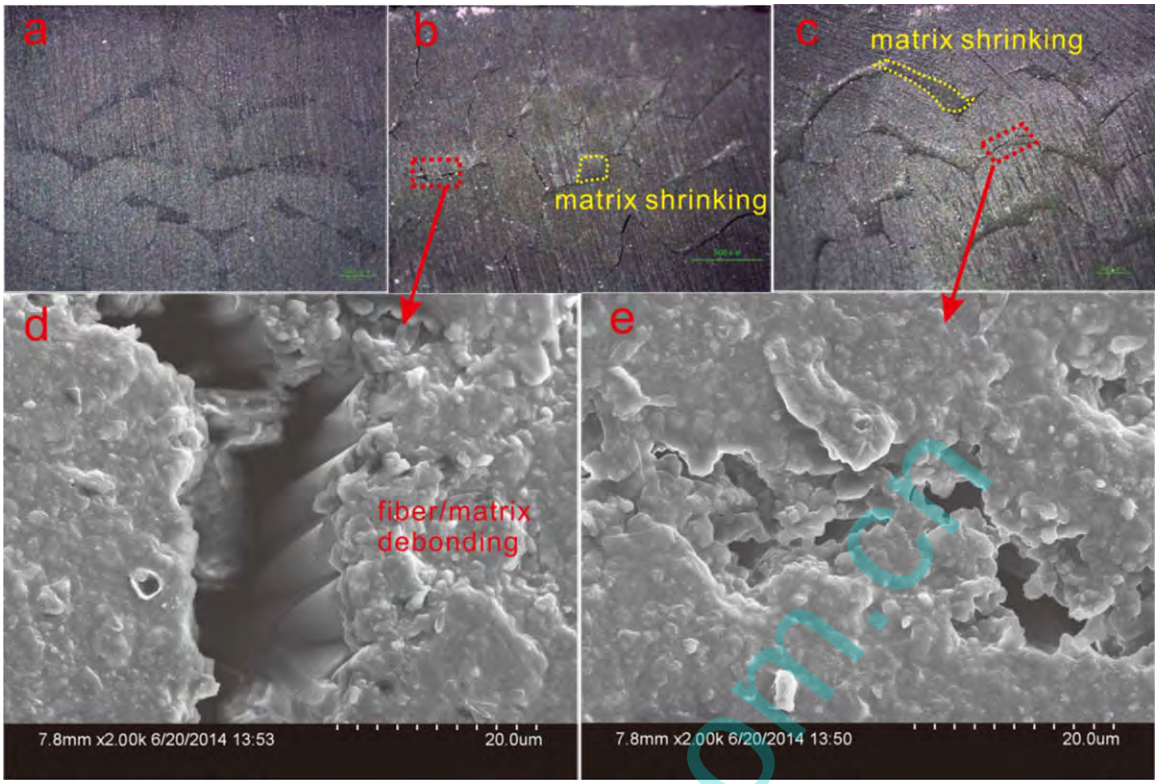

FIG. 11. Photomicrographs of cross-sections of (a) unaged and aged (1200 h at 140 °C) BC (b) and BGC (c); (d) Zoom on thermo-oxidation induced microcracks corresponding to (b); and (e) Zoom on thermo-oxidation induced microcracks corresponding to (c). [Color figure can be viewed in the online issue, which is available at wileyonlinelibrary.com.]

$$f = \frac{1}{2\pi}\left(\frac{1.875}{L}\right)^2\sqrt{\frac{EI}{\rho A}} \quad (1)$$

where L is the free length of the beam, E is Young's modulus, ρ is density, and A and I are the cross-section's area and moment of inertia. As the cross section is rectangular, the moment of inertia is $I = bh^3/12$ and the area is $A = bh$, where b and h are the width and thickness of the beam cross-section. Assuming a rectangular cross section, the above Eq. *1* can be rewritten as

$$f = \frac{h}{4\sqrt{3}\pi}\left(\frac{1.875}{L}\right)^2\sqrt{\frac{E}{\rho}} \quad (2)$$

The three composite beams had the same fiber volume fractions and specimen sizes, so their ρ can be considered to be equal to each other. At this time, the above Eq. *2* can be rewritten as: $f \propto \sqrt{E}$. For the unaged specimens, the theoretical E can be calculated using composite micromechanics approach [16, 24]. The theoretical E for BC and LC was 36.8 and 21.2 GPa, respectively. The $\sqrt{E_{BC}/E_{LC}} = 1.32$ was approximately equal to $FNF_{BC}/\ FNF_{LC} = 93.98/69.37 = 1.35$. For the unaged BGC, its FNF (99.01 Hz) was bigger than that of BC (93.98 Hz), which may be because the gradient stiffness made the gradient interphase act as a stress transfer medium and the load can be transferred from epoxy to carbon fibers uniformly, improving its E.

Four primary mechanisms have been suggested to contribute to damping in composites: viscoelastic response of the constituents, friction and slipping at the fiber matrix interface, thermoelastic damping because of cyclic heat flow and energy dissipation at cracks and delamination produced at damaged locations [25, 26]. Excluding the contribution from any cracks and other defects, the internal damping of a composite was determined by the following variables: properties and relative proportions of the matrix and the reinforcement; dimensions of the inclusions; orientation of the reinforcement with respect to the loading axis; surface treatments of the reinforcement and void content. The BC and LC had the same constituents and fiber volume content, so the difference of their FDC can only be attributed to the difference between the reinforced structures. For LC, the E with respect to the loading axis was significantly less than that of BC, so the FDC of the unaged LC (2.46%) was 0.48% higher than that of BC (1.98%). However, the FDC of BC was 0.13% higher than that of BGC (1.85%) because of the gradient interphase composed of GN and epoxy. Previous work [27] shows that low adhesion between fiber and matrix has an important effect on loss factors, because the low interface stiffness causes a redistribution of the elastic strain energy, resulting in a greater

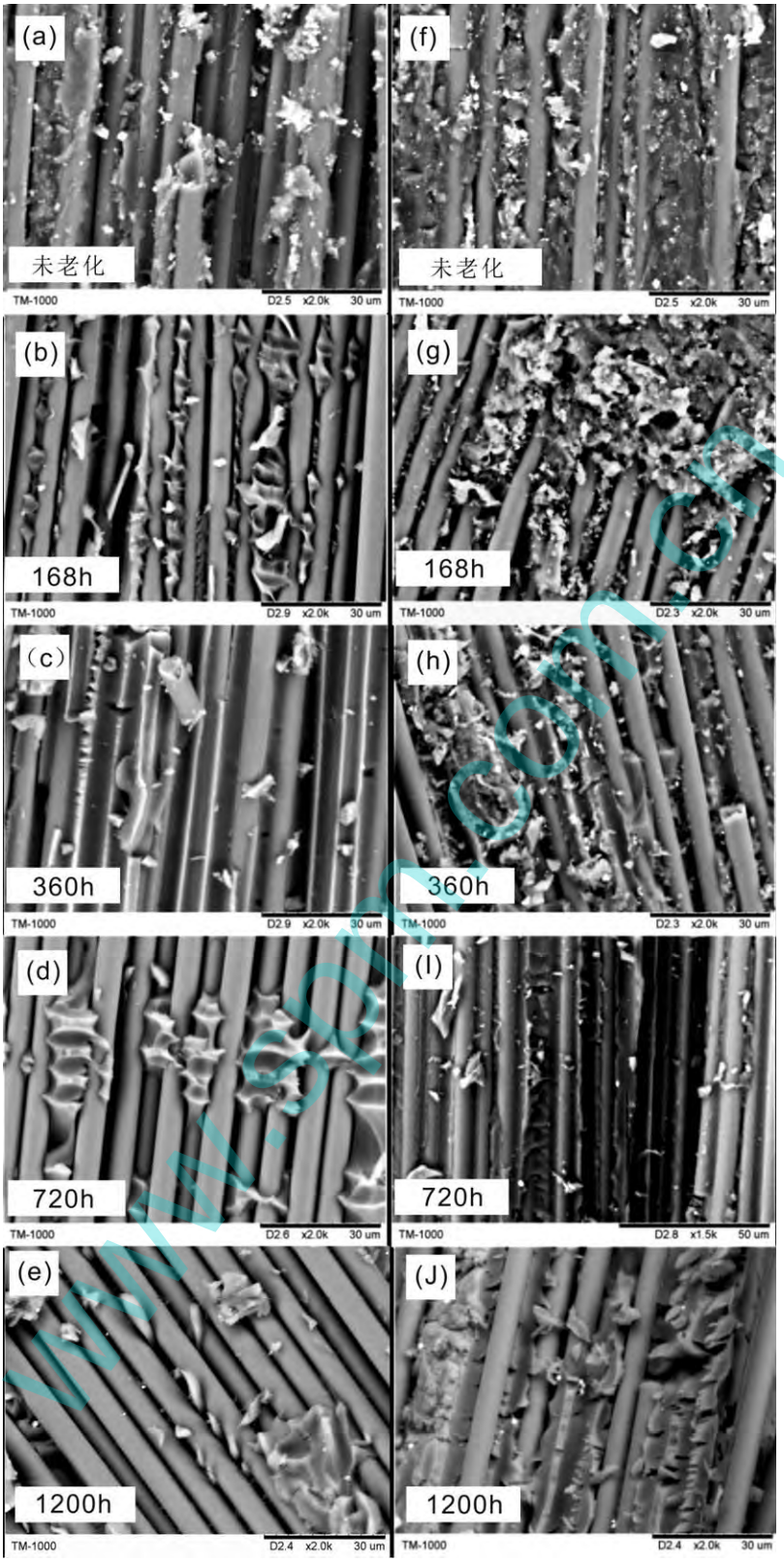

FIG. 12. SEM pictures of the fracture surfaces of unaged and aged (1200 h at 140 °C) BC (left) and BGC (right).

contribution from interface damping. GN produced by thermal reduction of graphite oxide [28] had residual hydroxyl and epoxide functional groups which could interact covalently with the epoxy chains, promoting interfacial adhesion, so the interface damping of BGC was lower than that of BC.

 DOI 10.1002/pc

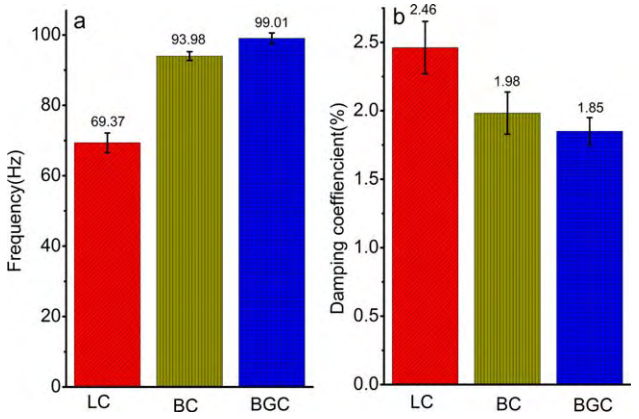

FIG. 13. (a) The first natural frequency and (b) the first damping coefficient of the three unaged composites. [Color figure can be viewed in the online issue, which is available at wileyonlinelibrary.com.]

After exposure to 140 °C, the FNF decreased and FDC increased with the increasing of aging time for the three composites. From Eq. *2*, it can be understood that the decreases in the FNF can occur when either density was increased or Young's modulus was decreased. When density was measured, there was no difference within the error bounds. Therefore, the decrease of FNF was because of the decrease of E. And the decrease of E was indirectly confirmed by the decrease of E' (Fig.9a). The microcracks (Figs. 10 and 11) and the degradation of fiber/matrix interface properties (Fig. 12) caused by TOA should be responsible for the increase of the FDC, because the energy was dissipated at the microcracks locations in composites.

At the same aging condition, the decrease in FNF and the increase in FDC of LC were higher than those of BC. It was because the LC lost more weight than that of BC at the same aging condition, and the more weight loss was because of the more serious fiber/matrix interface oxidative damage. The decrease in FNF and the increase in FDC of BGC were less serious than those of BC. It was because the GN reinforced gradient interface had effectively reduced the interface damage. This effect for GN, likely because of several reasons: (1) GN produced by thermal reduction of graphite oxide [28] had residual hydroxyl and epoxide functional groups which could interact covalently with the epoxy chains thereby further promoting interfacial adhesion, which can prevent oxygen from penetrating deep into the composite along the fiber/matrix interface during the aging process, reducing the interface oxidation; (2) The axial [100 W/(m·k)] and radial thermal conductivity [11 W/(m·k)] of T700 carbon fiber [29] were 555 and 61 times as high as those of neat resin [0.18 W/(m·k)], respectively. Mismatches in the thermal conductivity between the fiber and matrix give rise to localized thermal stress at the fiber–matrix interface, which are prone to induce microcracks. After adding GN at the fiber–matrix interface in carbon fiber/epoxy composites, the thermal conductivity of BGC was improved by 13% compared to BC. The carbon element content dwindled steadily from carbon fibers to epoxy (Fig. 5d) indirectly indicating that the thermal conductivity of the GN-reinforced gradient interphase layer was lower than that of carbon fiber and higher than that of matrix. The gradient conductive layer might transfer the

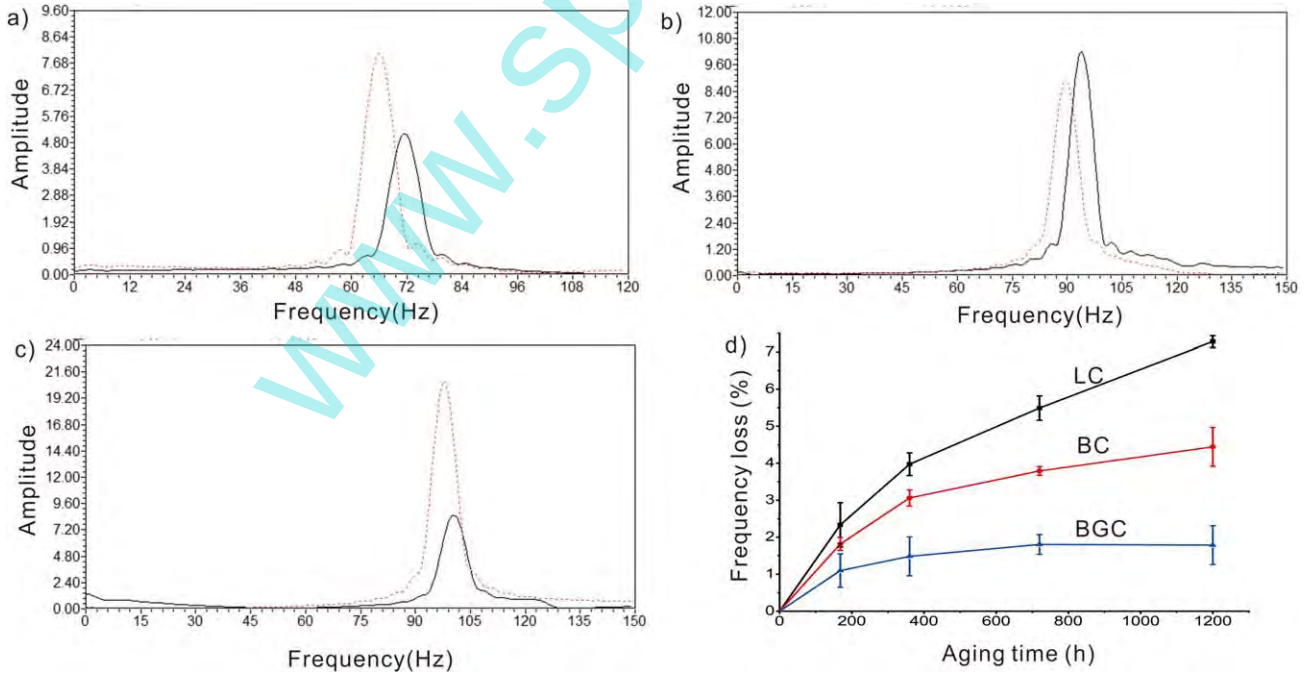

FIG. 14. Frequency response functions of the aged (a) LC, (b) BC, and (c) BGC specimens compared to unaged ones. (d) The FNF retention rate vs. aging time for specimens aged at 140 °C. [Color figure can be viewed in the online issue, which is available at wileyonlinelibrary.com.]

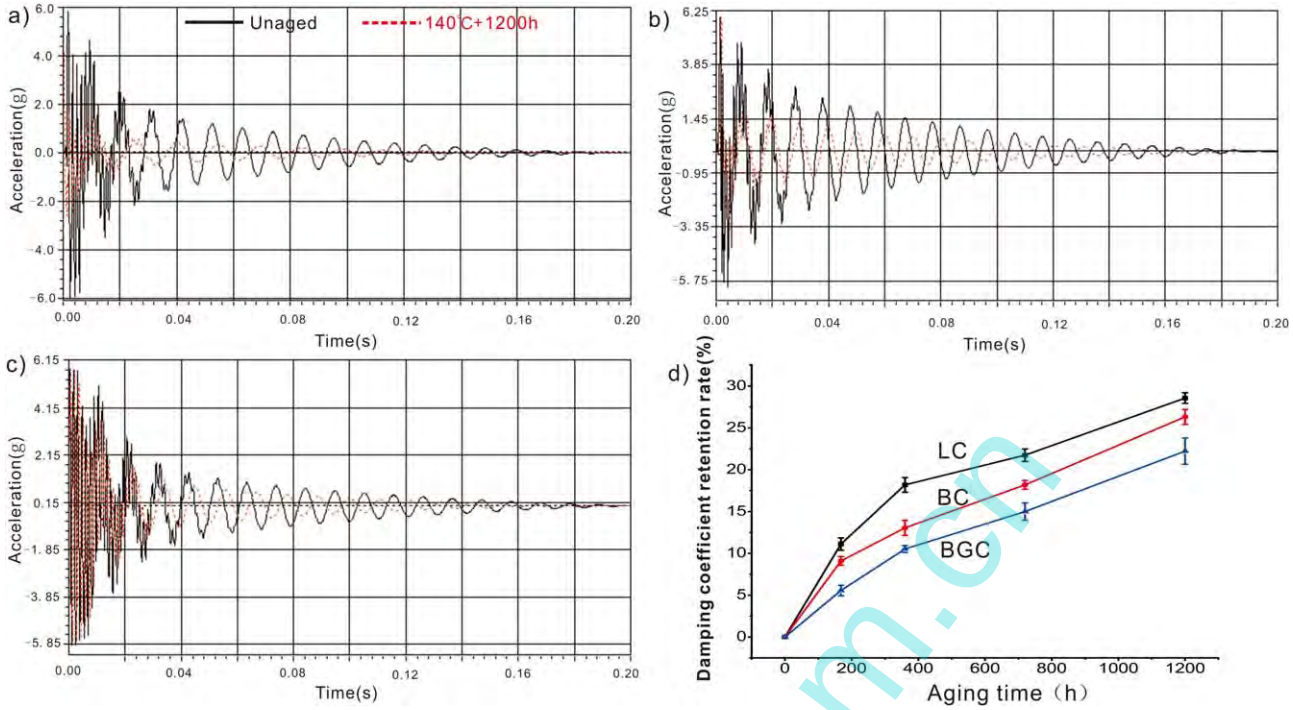

FIG. 15. Damping behavior curves of the aged (a) LC, (b) BC, and (c) BGC specimens compared to unaged ones. (d) The FDC retention rate vs. aging time for specimens aged at 140 °C. [Color figure can be viewed in the online issue, which is available at wileyonlinelibrary.com.]

interfacial thermal stress, mitigating the interface damage; (3) The specific surface area (>700 m^2/g), the micron size dimensions, high aspect-ratio and two-dimensional sheet geometry of GN made it highly effective at hindering the propagation of microcracks [9]; (4) Thee rough and wrinkled surface topology of GN can enable it to mechanically interlock, restricting the movement of the different phase of the materials at the composite interface although the adhesive force between fiber bundles and resin decreased after long time accelerated aging at high temperature.

CONCLUSIONS

In this study, the effect of thermo-oxidative aging on the vibration damping characteristics of the conventional fabric composites reinforced by three dimensional (3D) and four directional (4Dir) braided preform and laminated plain woven fabric and the 3D-4Dir braided graphene-based carbon fiber composites was investigated. It was found that the thermo-oxidative aging resulted in deterioration of the matrix and interface performance, in the form of weight loss, shrinking, microcracks and fiber/matrix debonding, which should be responsible for the decrease of nature frequency and the increase of damping coefficient of the composites. However, the first nature frequency (FNF) and first damping coefficient (FDC) retention rates for the three composites were different. For example, after exposure to 140 °C for 1,200 h, the FNF and FDC retention rates of 3D-4Dir braided graphene-coated carbon fiber/epoxy composite were 5.5% and 6.4% higher than those of laminated composite, respectively. One of the reasons was the integrated structure of 3D-4Dir braided composite exposed lower fiber end area to air than that of laminated composite, leading to less interface oxidation. Another reason was that the graphene nanoplatelet (GN) reinforced gradient interphase may provide an effective shield against interface oxidation and restrict the movement of the different phase of the materials at the composites interface. These results demonstrated that the 3D-4Dir braided structure and GN reinforced gradient interface had an obvious synergetic reinforcing effect on the vibration damping characteristics of carbon fiber reinforced polymer composites (CFRPCs), which provides an easy and effective way to design and improve the durability, safety and reliability of CFRPCs that are increasingly the material of choice in the aerospace industry. As Young's modulus and the natural frequency of the material have a strict mathematical relationship, the modal analysis technique might be performed in a nondestructive manner to understand the mechanical property of the CFRPCs after thermo-oxidative aging, and it will be studied in the future.

REFERENCES

1. X.L. Yang, Z.C. Wang, M.Z. Xu, R. Zhao, and X.B. Liu, *Mater. Des.*, **44**, 74 (2013).
2. C. Zhang, W.K. Binienda, G.N. Morscher, R.E. Martin, and L.W. Kohlman, *Compos. Part A*, **46**, 34 (2013).

3. H.J. Zo, S.H. Joo, T. Kim, P.S. Seo, J.H. Kim, and J.S. Park, *Fiber. Polym.*, **15**, 1071 (2014).
4. W. Fan and J.L. Li, *Polym. Compos.*, **35**, 975 (2014).
5. D.Q. Vu, M. Gigliotti, and M.C. Lafarie-Frenot, *Compos. Part A*, **44**, 114 (2013).
6. M.H. Haque, P. Upadhyaya, S. Roy, T. Ware, W. Voit, and H. Lu, *Compos. Struct.*, **108**, 57 (2014).
7. D.S. Li, D. . Fang, G.B. Zhang, and H. Hu, *Mater. Des.*, **41**, 167 (2012).
8. K.J. Bowles, M. Madhukar, D.S. Papadopoulos, L. Inghram, and L. McCorkle, J. Compos. *Mater.*, **31**, 552 (1997).
9. F. Yavari, M.A. Rafiee, J. Rafiee, Z.Z. Yu, and N. Koratkar, *ACS Appl. Mater. Interfaces*, **2**, 2738 (2010).
10. X. Zhang, X. Fan, C. Yan, H. Li, Y. Zhu, X. Li, and L. Yu, *ACS Appl. Mater. Interfaces*, **4**, 1543 (2012).
11. M.T. Kim, K.Y. Rhee, I. Jung, S.J. Park, and D. Hui, *Compos. Part B*, **63**, 61(2014).
12. Akay M, Spratt G. *Compos. Sci. Technol.*, **68**, 3081(2008).
13. D.C. Marcano, D.V. Kosynkin, J.M. Berlin, A. Sinitskii, Z. Sun, A. Slesarev, L.B. Alemany, W. Lu, and J.M. Tour, *ACS Nano*, **4**, 4806 (2010).
14. L. Chen, H. Jin, Z.W. Xu, M.J. Shan, X. Tian, C.Y. Yang, Z. Wang, and B.W. Cheng, *Mater. Chem. Phys.*, **145**, 186(2014).
15. L. Chen, Ph. D. Dissertation, Tianjin Polytechnic University, 2013.
16. X. Sun and C.J. Sun, *Compos. Struct.*, **65**, 485 (2004).
17. J. Wolfrum, S. Eibl, and L. Lietch, *Compos. Sci. Technol.*, **69**, 523 (2009).
18. Y.M. Pei, K. Wang, M.S. Zhan, W. Xu, and X.J. Ding, *Polym. Degrad. Stab.*, **96**, 1179 (2011).
19. S. Ohno, M.H. Lee, K.Y. Lin, and F.S. Ohuchi, *Mater. Sci. Eng. A*, **293**, 88 (2000).
20. M.A.B. Meador, C.E. Lowell, P.J. Cavano, and P. Herrera-Fierro, *High Perform. Polym.*, **8**, 363 (1996).
21. K.S. Kumar, I. Siva, P. Jeyaraj, J.T.W. Jappes, S.C. Amico, and N. Rajini, *Mater. Des.*, **56**, 379 (2014).
22. G. Schoeppner, G. Tandon, and E. Ripberger, *Compos. Part A*, **38**, 890 (2007).
23. L. Meirovitch, *Analytical methods in vibration*, Ccollier-MacMillan Ltd., London (1967).
24. R. Wang, J.K. Wang, and L. Wu, *Acta Mater. Compos. Sin.*, **19**,90 (2002).
25. E.C. Botelho, M.L. Costa, L.C. Pardini, and M.C. Rezende, *J. Mater. Sci.*, **40**, 3615 (2005).
26. A. Etaati, S.A. Mehdizadeh, H. Wang, and S. Pather, *J. Reinf. Plast. Compos.*, **33**, 330 (2014).
27. J. Vantomme, *Composites*, **26**, 147 (1995).
28. D.A. Dikin, S. Stankovich, E.J. Zimney, R.D. Piner, G.H.B. Dommett, G. Evmenenko, S.T. Nguyen, and R.S. Ruoff, *Nature*, **448**, 457 (2007).
29. J. Schuster, D. Heider, K. Sharp, and M. Glowania, *Compos. Sci. Technol.*, **68**, 2085 (2008).